Supporting Information

Readily Constructed Glass Piston Pump for Gas Recirculation

Adam C. Nielander[1], Sarah J. Blair[1], Joshua M. McEnaney[1], Jay A. Schwalbe[1], Tom Adams[2], Sawson Taheri[3], Lei Wang[1], Sungeun Yang[4], Matteo Cargnello[1], Thomas F. Jaramillo*[1]

[1]Department of Chemical Engineering, Stanford University

443 Via Ortega, Stanford, California 94305, United States

[2]Adams & Chittenden Scientific Glass

2741 Eighth St., Berkeley, California, 94710, United States

[3]Stanford Prototyping Facility, Stanford University

350 Jane Stanford Way, Stanford, California, 94305, United States

[4] Department of Physics, Technical University of Denmark, Building 311, Fysikvej, DK-2800 Kgs. Lyngby, Denmark

*Corresponding Author; email: jaramillo@stanford.edu

Table of Contents

Associated Files (In 'Additional_SI_Files.zip'):

1. Solidworks_Part_Files
   a. Piston Body.SLDPRT;
   b. Piston Screw Cap.SLDPRT;
   c. Stir Magnet.SLDPRT;
   d. Piston Screw Cap and Magnet.SLDASM
2. SI_Movie_1_and_2
   a. SI_Movie1_Operation1_6in_100mLmin_SI.mp4
   b. SI_Movie2_Operation2_LowFlow_Recirculation_SI.mp4
3. Table_of_Glass_Pump_Components.xlsx
4. Pump_Controller_No_Ext_Control.txt

Construction of Glass Pump

The glass body of the pump was fabricated by Adams & Chittenden Scientific Glass (Berkeley, CA) and is available for purchase. A schematic diagram of the pump, including dimensions, can be seen in Figure S1. The magnetic PEEK piston was fabricated by inserting a PEEK-encapsulated, NdFeB magnet (V&P Scientific, San Diego, CA) into a custom-machined, sealable PEEK piston body. The piston body was sealed with a PEEK screw cap to complete the piston. A schematic of the PEEK piston body can be seen in Figure S2, and design files (Solidworks 2018, Dassault Systemes) of the screw cap, magnet, and piston body are provided (Piston Body.SLDPRT; Piston Screw Cap.SLDPRT; Stir Magnet.SLDPRT; Piston Screw Cap and Magnet.SLDASM). We note that the interior portion of the piston body was machined to match the as-received stir magnet to account for variability in the stir magnet dimensions. The outer rings of the piston body were also machined to slightly larger than 19 mm and then carefully sanded with 600 grit sandpaper to mate the piston rings to the 19 mm diameter of the piston tube. The 1.5 mm diameter through hole in the end of the piston body was used to assist in retrieving the piston body from the piston tube during this process. A small, 10 mm x 10 mm x 5 mm piece of PTFE ('anti-wedge stopper') was inserted into the piston tube to inhibit the piston from seizing near the end of the piston tube as a result of the closely matched diameters of the piston ring and piston tube. A threaded PTFE tube screwed into a small, tapped hole in the Ace Thred #25 PTFE plug was also optionally used to keep the piston within the piston tube though this was generally achievable with software control. A back-sealed FETFE o-ring was used in conjunction with the Ace Thred plug. The magnet coils were manually wound using 20 AWG copper magnet wire (TEMCo Industrial, Fremont, CA) and adhered using cyanoacrylate adhesive with an adhesive accelerator to quickly harden the adhesive. Each magnet coil consisted of 1000 turns of wire (windings) with a total width of approximately 41 mm and an inner diameter of approximately 43.5 mm. An extended description of the coil fabrication is associated with Figure S3 and Figure S4. Fabrication of the magnet coils was found to be the most labor-intensive step in the pump fabrication, but custom magnet coils can instead be readily purchased from a number of suppliers, including

Custom Coils, Inc. (Benicia, CA).The diameter was selected such that the magnet coils could snugly but freely slide past the glass diameter of the Ace Thred #25 and into the 'installed' position. A layer of thermal insulation tape (010120 Exhaust Heat Wrap; Design Engineering, Inc., Avon Lake, OH) secured with Kapton tape (Polyimide Film Tape 5413, 3M) was used to match the diameter of the outer piston tube to the magnet coils and inhibit heat transfer from the active magnet coils to the recirculating gases during operation (See Figure S5a). During operation, the pump was held in place using three standard large (grip size ≥4 inches) three-prong laboratory clamps (note: a wide variety of stabilizing strategies should be effective). The clamping mechanism is visible in Figure S5c and S5d. The weight of the magnet coils dictated that the stabilizing mechanism primarily support the weight of the magnet coils. Images of selected pump components can be seen in Figure S5. An image of the pump in a subset of the operating conditions shown in Table 1 can also be seen in Figure S5. Two movies showing pump operation are also provided: SI Movie 1 (SI_Movie1_Operation1_6in_100mLmin.mp4) and SI Movie 2 (SI_Movie2_Operation2_LowFlow_Recirculation.mp4). SI Movie 1 shows the pump operating at a flow rate of approximately 100 mL min^{-1} against a pressure of 6" H_2O. SI Movie 2 shows the pump operating at a low flow rate under recirculation with an exaggerated piston movement to demonstrate the pump operating mechanism. SI Movie 1 additionally includes a still frame of the power supply reading in the bottom left corner. The actual power supply output displays some variability with time.

Pump Operation and Control

The crucial requirement for pump operation is straightforward: the magnet coils must be variably powered in such a way that the piston moves to effect gas flow in a reactor. This can be achieved in myriad ways using the combination of the glass pump body, magnetic piston, and magnet coils described herein. Below we describe one strategy we have used to control the operation of the glass piston pump, but it is not the only or necessarily always most ideal method for pump operation and component selection. The critical need in unidirectional gas recirculation is an appropriately designed scheme of valves that enforce the desired unidirectional flow. Commercially available pumps, including diaphragm pumps and bellows pumps, are also useful when gas recirculation is needed, and potential users should explore such options. For our intended applications, we did not find commercially available solutions that directly met our required specifications (leak tightness, chemical compatibility, controllable/variable flow rate magnitude, user serviceability). We have found that the ability, in a laboratory environment, to directly optimize and to service the glass pump is also highly advantageous while doing exploratory work with a wide range of conditions (e.g., the glass pump components and seals can easily be cleaned or replaced).

The glass pump operation was controlled using a microcontroller (Arduino UNO Rev3, ATmega328P) coupled to a L298N dual H-bridge motor driver module and a variable 60 V, 1.5 A power supply (Protek 3006B; Protek Devices, Tempe, AZ). An example wiring diagram and brief description of the wiring can be found in Figure S6. Control of the pump operating characteristics were achieved by both software and hardware variable tuning. The tunable hardware variable was the power input/applied current as controlled directly by the power supply. The tunable software variables were the current input to each magnet coil (controlled by pulse width modulation) and the frequency of the voltage polarity switching as seen in the code in the provided file (Pump_Controller_No_Ext_Control.txt; note this code was originally written to be executed as a *.ino in the Arduino Integrated Development Environment [IDE]). Tuning of the frequency as well as the absolute and relative currents to the magnet coils directly controls the magnitude and “time variability” (i.e., smooth/intermittency of flow)

of the gas flow rate. The microcontroller hardware and software may also be modified to accept input from potentiometers to enable easy tuning of the operating parameters. The peak power inputs reported herein were approximated by noting the maximum voltage and current readings and multiplying these values. However, as noted above, the frequency of the pumping action is a controllable parameter, and therefore during operation there were often significant 'rest' periods in which no current flowed. Therefore, the reported peak power inputs represent a higher limit of the total power input.

During operation, the pump was connected to the reactor using either PTFE (Ace Glass, Vineland, NJ) or Ultra Torr (Swagelok, Solon, OH) compression fittings. The plumbing and valving used during N_2 reduction chemistry has recently been reported (see Andersen, et al., Nature 2019, Extended Data Figure 4).[1]

The data in Table 1 were collected by setting the pump up as shown in Figure S7. The controlled variables were the peak power input and differential pressure, where the differential pressure is reported as the pressure at the pump outlet relative to pressure at the pump inlet. As seen in Figure S7 and in SI Movie 1, the differential pressure was controlled by enforcing the depth of a tube attached to the pump outlet in a graduated cylinder filled with water. The inlet pressure was fixed at atmospheric pressure by leaving the inlet open to ambient conditions. The ability of the gas in the outlet tube to push the water level down was used to measure the pressure of the gas within the tube and was readily reported in pressure units of 'inches of H_2O' (1 in. $H_2O \approx$ 2.48 mbar). A flowmeter (Series VF Visi-Float Acrylic Flowmeter, Dwyer Instruments) in series with the outlet tube was used to measure the gas flow at an associated pressure. As seen in Table 1, for a given peak power input, the flow decreased as the outlet pressure increased (Figure S7 b,c,d). This is consistent with an increased resistance to piston movement as it encounters a larger pressure gradient across the piston. The pressure at which no flow is observed is a rough approximation of the maximum pressure gradient against which the piston can move at a given peak power input. The power input was increased by increasing the current/voltage output at the power supply. The increased current through the magnet coils generates larger forces between the

magnetic piston and the coils, allowing the piston to move faster and against larger pressure differentials. This can be seen in Table 1, where an increase in peak power input from 10 to 15 W (Figure S7d,e) increases the maximum observable pressure from 10 to 12 in. H_2O.

Leak Rate Analysis and Closed-Loop Recirculation Considerations

Minimizing the leak rate in recirculating gas experiments is imperative. We tested the leak rate of this glass piston pump using both a 'bubble' test and a 'pressure drop' test.[2] The 'bubble' test was executed in the following way: (1) the inlet and outlet of the pump were attached to each other using 1/8" OD FEP tubing (IDEX Corporation, Lake Forest, IL) and 1/8" to ½" PTFE compression fittings (Ace Glass). (2) The pump apparatus was pressurized to 30 in. H_2O with N_2 gas. At this point, the entirety of the pump apparatus was submerged in a water bath. No bubbles were observed, which is consistent with a leak rate $<10^{-3}$ mbar L s^{-1}.[2] A 'pressure drop' test was executed twice, once using Ultra Torr (Swagelok) connectors to connect the pump inlet and outlet using steel tubing and separately using PTFE compression fittings to connect the inlet and outlet using FEP tubing. In each case, a pressure gauge (0-60 in. H_2O range) was used to monitor the pressure in the tubing. The pressure in the pump was monitored over the course of 40 hours with the Ultra Torr connectors installed. After 40 hours, the pressure had dropped no more than 4 in. H_2O, corresponding to a leak rate of approximately 5 x 10^{-6} mbar L s^{-1} assuming a total system volume of 100 mL. The pressure in the pump was monitored over the course of 20 hours with the PTFE connectors installed. Over this time period, the pressure dropped to approximately 7 in. H_2O. A nearly linear leak rate of 9.0 x 10^{-5} mbar L s^{-1} was observed. We attribute the observed gas loss to leaks at the connections between the pump and the line and gauge as well as permeation through polymer components. We also note that dissolved gases, including O_2, may be dissolved in polymer components. Dissolved gases should be addressed and possibly removed via purging, evacuation (at room temperature or under heating), or other means.

Prior to executing an experiment, the air content in the pump body/sealed reactor should be removed via inert gas purge and/or reactor evacuation (See Figure S8). We have found five cycles of evacuation to 10 mbar followed by refill with argon at atmospheric pressure to be useful baseline method. While the glass pump described herein is capable of withstanding evacuation, special care should always be taken when evacuating or pressurizing glass components. Always inspect the glass for damage prior to use. Taping glass components or using a wire mesh can also mitigate the risk of injury from implosion. In addition to the evacuation/refilling process prior to experiment, the polymer-based components were treated to minimize O_2 and H_2O outgassing into the reactor (see below).

Accounting for and avoiding ingress of impurities or undesired reactants in a sealed reactor during reaction is also crucial. For example, in an unseparated (i.e., no membrane between cathode and anode) electrochemical cell, O_2 formation at the anode can quickly add significant O_2 content to the gas headspace. In the glass pump architecture described herein, polymer components and seals are an additional possible route for impurity (e.g., O_2, H_2O) introduction into the cell.

PTFE is known to contain significant amounts of O_2 when in equilibrium with air (~40 µL per cm^3_{PTFE}).[3] If we approximate the PTFE Ace Thred #25 plug to be 40 cm^3 of PTFE and an average reactor volume to be 0.1 L, the complete transfer of O_2 into the reactor volume would account for >1% of the total gas content and render the reactor headspace incompatible with oxygen-sensitive conditions. While the complete transfer of the PTFE-dissolved O_2 into the reactor headspace is highly unlikely on the timescale of an electrochemical reaction, this calculation serves as motivation to analyze how to minimize the introduction of impurities into the reactor.

Gases, including both O_2 and H_2O, may be inadvertently introduced into a reactor via a polymer component outgassing as noted above. There is a broad body of literature that considers the behavior of various gases with various polymers, with a particular focus on the compatibility of polymers in vacuum systems.[4–6] While an assessment of the rate of transfer of a molecule of interest through a polymer component/seal is most accurately determined experimentally, we have used previously reported data on

polymer-gas interaction characteristics to inform our design of practices to avoid O_2 and H_2O.

We first consider outgassing from PTFE after air exposure. Outgassing rates have been previously measured to be approximately 5 x 10^{-8} mbar L s^{-1} cm^{-2} after three hours under evacuation with the majority of the gas being N_2 and an approximate contribution from O_2 of 1.3 x 10^{-9} mbar L s^{-1} cm^{-2}.[7] For a 0.1 L reactor volume, a 10 cm^2 PTFE seal, and an initial pressure of 1075 mbar, this level of outgassing would increase the O_2 concentration approximately 1.5 ppm O_2 per hour assuming no loss of gas from the reactor headspace. While this rate of O_2 ingress into the reactor may be acceptable, we noted that other reports on PTFE outgassing had observed up to an order of magnitude higher outgassing rates (though the contribution to the total outgassing from the various components of the gas composition, i.e., outgassing due to N_2 and O_2 were not reported separately, was not reported). In order to minimize the rate of outgassing of PTFE, we have found baking the PTFE Ace Thred plug under vacuum to be useful. This is a common strategy when using polymer seals in vacuum equipment. While we were unable to find a report that exactly studied the effect of vacuum baking on the outgassing rate of PTFE, we did find literature evidence that a similar strategy can reduce the outgassing rate of Viton o-rings by five orders of magnitude (down to 2.7 x 10^{-10} mbar L s^{-1} cm^{-2}).[4] Further, related studies on the vacuum baking of PTFE have shown promising results, and baking of PTFE plugs has been advertised by Ace Glass as a method to greatly reduce achievable vacuum levels (see Ace Glass Document F1022, 11/2017).[8] We ultimately determined that a 100 °C bake under vacuum for ≥ 4 hr should be effective under standard conditions. At 100 °C, the diffusion constant for O_2 in PTFE is increased by an order of magnitude (D_{25C} = 1.52 x10^{-7} cm^2 s^{-1}; D_{100C} = 1.33 x 10^{-6} cm^2 s^{-1}), which leads the vacuum baking strategy to deplete the PTFE of O_2 to a sufficient depth that the O_2 level would not immediately return to the air-saturated level when manipulated in ambient conditions.[3,9] A similar process should be useful when using polymer compression seals at the inlet and outlet of the pump. We also used a similar baking procedure to remove H_2O and O_2 from the PEEK components.[10] It is important to note that the magnet used here has a maximum operating temperature

of 80 °C and therefore was exposed to vacuum but was not heated. PEEK-coated magnets with identical dimensions but with higher maximum operating temperatures are commercially available as required.

While the rate of impurity ingress can be reduced using various strategies, there are experimental conditions in which any impurity ingress may not be compatible with the reaction of interest and can be further mitigated by operating in a glovebox or by replacing the internal Ace Thred/PTFE seal with an alternate seal, such as an Ace Thred Plug with a front seal, a glass-to-KF flange (available from Ideal Vacuum Products, Albuquerque, NM, USA) or an NW glass flange (available from Adams & Chittenden, designed for high vacuum use). These modifications may require glassblower manipulation of glass components.

Gas headspace composition considerations

The composition of the gas in the headspace of a closed-loop recirculating/sealed reactor may reasonably be expected to be a function of both the Faradaic efficiency and applied current of an electrochemical reaction. Understanding this interplay is important to predict the overall pressure of the headspace gas, to maintain the integrity/safety of the reactor, and to understand observed electrochemical behavior. For example, the co-evolution of H_2 at the cathode is often observed during attempted electrochemical N_2 reduction. If we assume a maximum safe pressure of 1.5 bar, an initial reactor pressure of 1.075 bar (slight overpressure to mitigate leaks into the reactor), gas ideality, and 100% Faradaic efficiency toward H_2, we can readily calculate the reaction time that would be required to reach this pressure as a function of current density using the equations below:

$$Q_{H_2} = i * t \qquad \text{(Eqn S1)}$$

$$n_{H_2} = \frac{Q_{H_2}}{2F} \qquad \text{(Eqn S2)}$$

$$\Delta P = \frac{i*t*RT}{2FV} = \ n_{H_2} * \frac{RT}{V} \qquad \text{(Eqn S3)}$$

$$\Delta P = P_{max} - P_0 \qquad \text{(Eqn S4)}$$

In the above equations, Q_{H2} is the total charge passed toward H_2, i is the applied current in the reactor, t is the reaction time, n_{H2} is the moles of H_2 produced, F is Faraday's constant (96485 C mol^{-1}), ΔP is the change in pressure, R is the ideal gas constant, T is the temperature of the reactor, V is the volume of the reactor, P_{max} is the defined maximum safe pressure, and P_0 is the initial reactor pressure. We note that the factor of '2' present in the denominator of equations S2 and S3 reflects the $2e^-$ passed to generate 1 molecule of H_2.

Using equation S3, and assuming ΔP=0.425 bar, T= 300 K, and, V= 0.1 L, we can see that $(i * t)$ is equal to 328.8 C. If we assume a reaction rate of 1 mA, we can readily translate this to a 'safe' reaction time of approximately 91 hours. This 'safe' reaction time will decrease as the total applied current increases; for example, at 100 mA, the total 'safe' reaction time decreases to less than 1 hour.

We can further generalize this argument by considering the concurrent formation of NH_3, which should reduce the pressure in the reactor by removing N_2. This assumes that all NH_3 formed remains in the solution phase (NH_3 solubility in H_2O = 31% w/w; NH_3 solubility in THF = 0.34 M)[11,12] :

$$\Delta P = \frac{i*FE_{H_2}*t*RT}{2FV} - \frac{i*FE_{NH_3}*t*RT}{3FV} \text{ (Eqn S5)}$$

Where FE_x is the Faradaic efficiency of the denoted product 'x'. As can be seen in equation S5, the sign of the pressure change will be a function of the relative Faradaic efficiencies observed for each reaction at the cathode. This analysis can be readily expanded to calculate partial pressures of each gas as a function of time if the initial composition of the reactor gas is known. The possibility of gas evolution or decomposition due to reaction at the anode (e.g. water oxidation to form O_2, H_2 oxidation to form H^+) are additional complicating factors and should be considered where relevant.

Maintaining a constant gas composition in a sealed reaction vessel is inherently challenging as all gaseous products formed are added to the headspace and the desired reactant is constantly removed from the headspace. As suggested by equation

S3, experiments that require high currents and low reactor volumes may be most affected by these constraints.

There may be situations in which it is desirable to add complexity in order to maintain a more constant composition in the gas headspace within a closed loop system. These challenges can be addressed through various means, including by selecting reaction-compatible absorbents to remove undesired products (e.g. H_2, O_2), adding reactant gas 'mid-run' for reactions in which the reactant gas reacts quickly, and increasing the total reactor volume relative to the current passed, among other possibilities. To address this issue, one may also consider strategies employed to address similar issues of gas headspace composition maintenance in industrial processes that use looped gas streams, including during industrial ammonia synthesis. During industrial ammonia synthesis, $H_{2(g)}$ separation from purge gas is useful, and separation methods based on selective membranes as well as carbon, polymer and metal/metal hydride-based absorbents have been devised.[13]

Applying these methods to the electrochemical looping strategy requires consideration of the similarities and differences between the headspace composition in the two processes. While the headspace gas in the industrial process has many of the same components as would be expected in an electrochemical looping experiment (H_2, N_2, NH_3), the electrochemical experiments are expected to also have significant quantities of solvent vapor (H_2O, organic solvent, etc. depending on reaction conditions) since the headspace should be saturated with the electrolyte solvent to prevent solvent loss in the cell over time. Additionally, the industrial process is expected to employ much higher gas pressures and temperatures than those in the electrochemical experiments that are enabled by the glass piston pump described herein.[13] These differences complicate the analysis necessary to propose methods for active H_2 removal since a significant portion of the previously reported experimental work was done to understand H_2 separation at these higher temperatures and pressures; however, we can nonetheless use available data to guide us toward effective H_2 separation methods under electrochemical looping conditions.[13–15] One proposed method is the incorporation of a thin Pd or Pd-Ag membrane in parallel with the gas

loop. These membranes have the advantage of exquisite selectivity for H_2 permeability compared to other H_2 separation methods.[15,16] Although many of the H_2 permeability studies of these membranes have been executed at higher temperatures and pressures, an extrapolation to room temperature and near ambient pressure suggests that the rate of H_2 flux across the membrane should be sufficient to remove H_2 at rates commensurate with expected H_2 generation at the cathode.[17] Additionally, Pd and Pd-Ag membranes are not strongly poisoned by the presence of NH_3 or N_2 in the stream.[17,18]

H_2 absorber materials that efficiently uptake H_2 and low H_2 partial pressure at ambient temperature may serve as another viable strategy for removing H_2 from a looped gas stream. A wide variety of H_2 absorber materials are known, and Pd and Pd-Ag, as well as other commercially available metal/metal hydride alloys such as $LaNi_5$, are promising as direct H_2 absorbers in these electrochemical looping experiments based on large solubility of H_2 in the materials.[16,19,20] Pd-based materials have demonstrated both facile kinetics and attractive equilibrium compositions between $H_{2(g)}$ and the absorbing metals at the relevant pressures and temperatures.[21] $LaNi_5$ has been studied as a hydrogen absorber for industrial ammonia purge gases, and is known to be stable in the presence of NH_3.[22]

Another possible strategy is the use of polymer or carbon-based selective H_2 membranes. These membranes selectively allow H_2 to permeate with respect to other gases, such as N_2, effecting gas separation. The imperfect selectivity of these membranes will allow some $^{15}N_2$ to escape the reactor in isotope-labeled experiments, and this issue can be relieved by a carefully metered addition of $^{15}N_2$ makeup gas into the reactor loop. A wide variety of polymer membranes have been characterized for their permeability to H_2 and separation factor for H_2 permeation with respect to other gases, and both of these factors should be considered when making a membrane selection. To understand the factors that dictate the required permeability and separation factor, we can consider an example system in which we are constantly passing 1 mA toward H_2 generation. This is approximately 5.2×10^{-9} mol H_2 s^{-1} added to the loop, or 1.16×10^{-4} mL H_2 s^{-1} (assuming gas ideality). At an H_2 pressure differential

of 0.425 bar (31.9 cm Hg) across the membrane, a membrane thickness of 0.01 cm, and a membrane area of 10 cm^2 would require permeability of ~36.4 barrer ($1\ \text{barrer} = 10^{-10}\ \frac{\text{cm}^3_{\text{STP}}\cdot\text{cm}}{\text{cm}^2\cdot\text{s}\cdot\text{cmHg}}$) to maintain a constant partial pressure of H_2. Based on the experimentally-defined relationship between permeability and separation factor, we expect the separation factor (H_2/N_2) to decrease as permeability to H_2 increases, with a maximum separation factor of ~100 for a permeability of 36.4 barrer.[23] Assuming this separation factor, we expect to observe an N_2 'leak' rate through the membrane of approximately 2.8 x 10^{-6} mL N_2, or less than 1 mL of N_2 lost per day. As noted above, this N_2 could be replaced through metered addition of N_2 to the gas loop to maintain a constant partial pressure. Composite polysulfone-based polymers have been used as H_2 separation membranes in industrial ammonia synthesis. One such polymer membrane, with a reported separation factor of ~39 and H_2 permeability of ~5370 barrer, is expected to remove H_2 at a much higher rate (and thus much lower steady state H_2 pressure) but is expected to pass N_2 at a rate of 0.001 mL N_2 s^{-1}, requiring ~86 mL per day to maintain partial pressure.[15,24] Membrane selection will depend on a number of factors, including rate of H_2 (or other gas) generation as well as stability to solvent vapors and NH_3.

Species that may poison the H_2 separation ability of these materials, such as NH_3 or an organic solvent, could be removed prior to H_2 using an in-line scrubber or cold trap. If the solvent vapor is removed, however, a method for re-introduction of solvent must be employed to maintain the solvent volume in the cell. Ultimately, the specific reaction conditions will dictate the correct set up, making *a priori* prescription of methods challenging. Because of the variety of considerations associated with sealed reactors, *active monitoring of the gas pressure is crucial* both for safety and to understand the reaction under study.

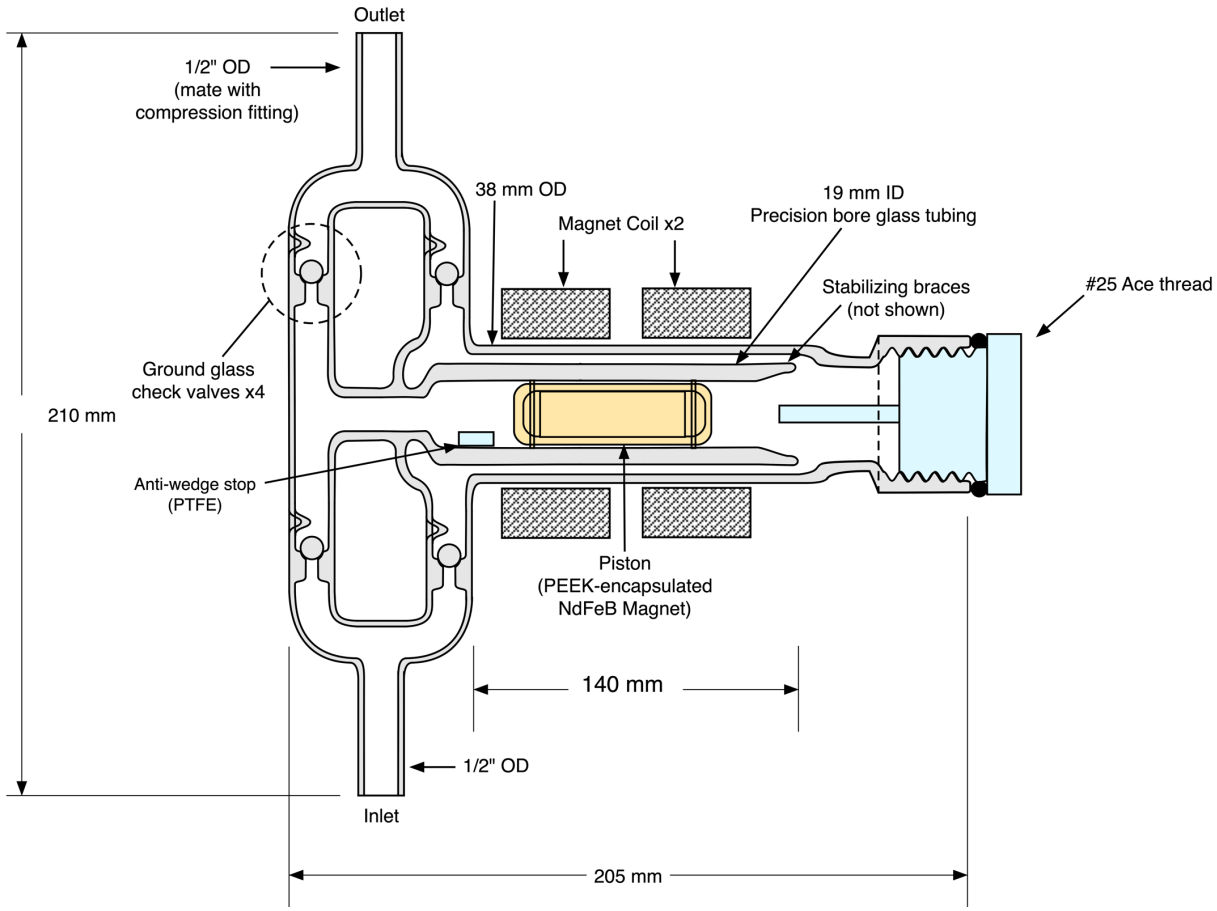

Figure S1: Schematic of the magnetically-actuated glass piston pump. Note the piston sits within the piston tube and the piston tube is positioned within the wider diameter tube ("gas-transfer tube"). Materials colored gray are made of glass. Glass walls are at least 'medium wall' thickness as defined by the relevant tube diameter. Materials made of PEEK are in yellow. Materials made of PTFE are colored blue. The copper magnet coils are crosshatched.

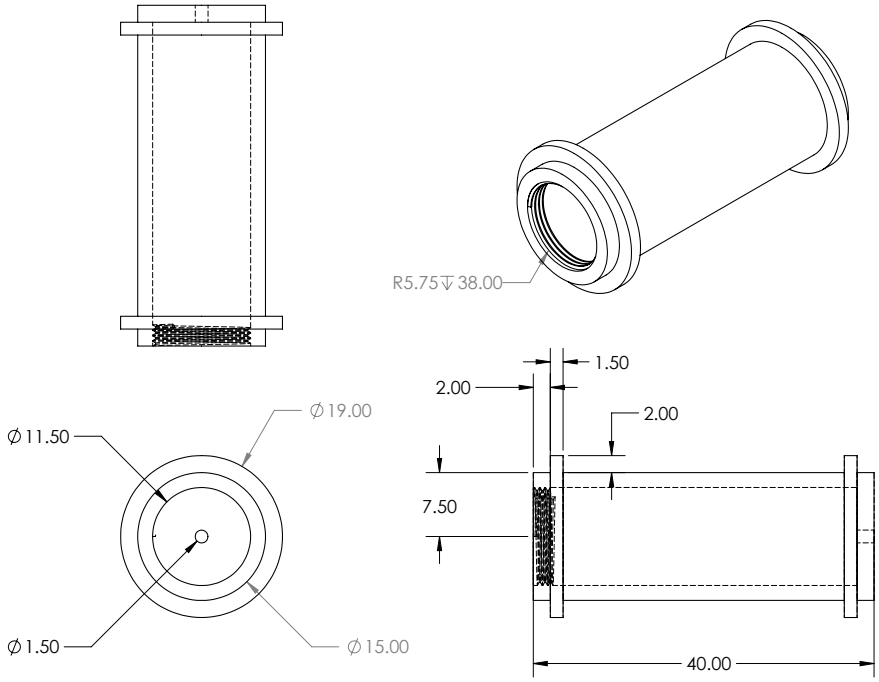

Figure S2: Schematic drawing of the piston body (Units – millimeters).

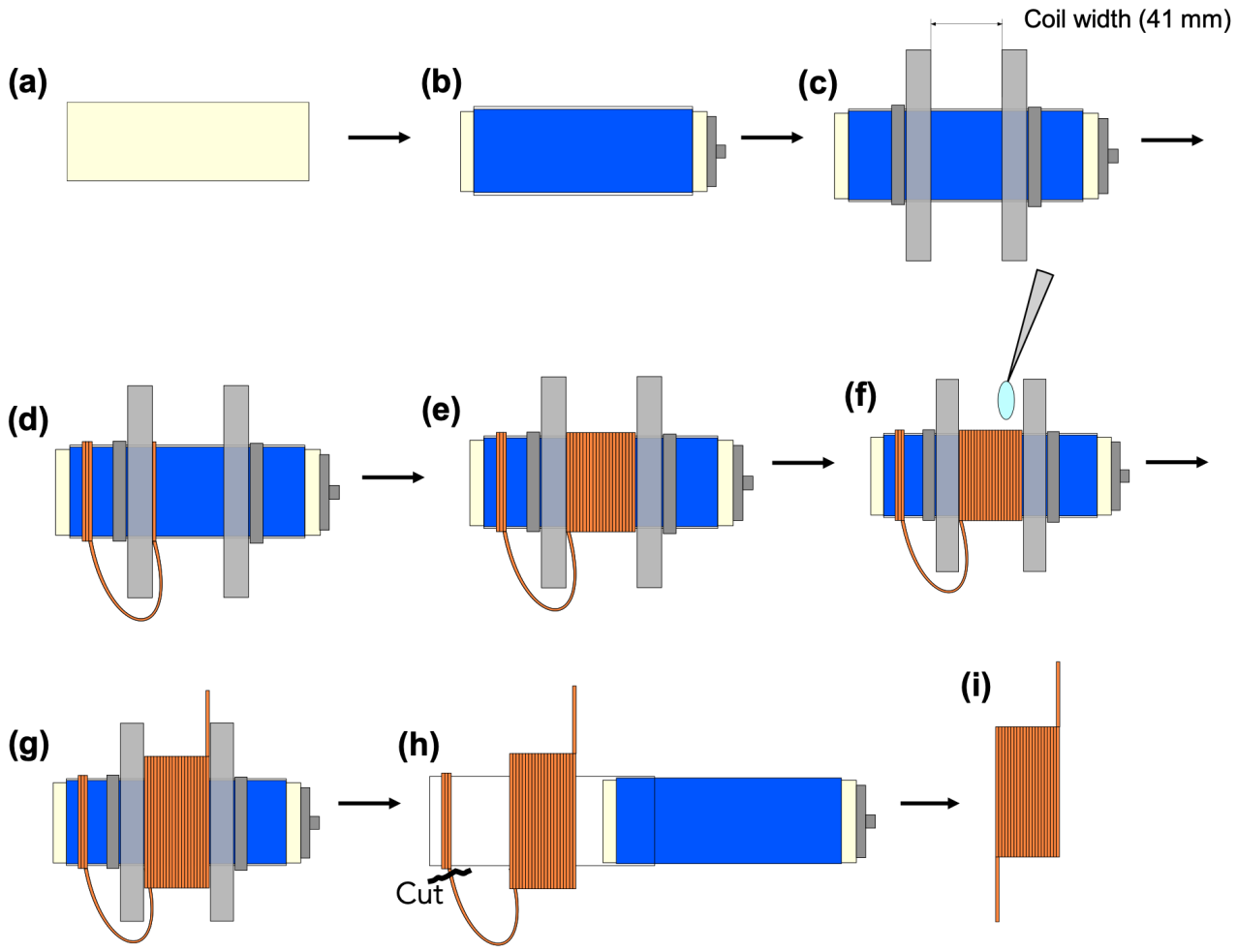

Figure S3: Schematic description of the copper magnet coil fabrication method used herein. Associated images of the steps above can be found below in Figure S4. A complete list of the parts and supplies used can be found in the associated spreadsheet file (Table_of_Glass_Pump_Components.xlsx) (a) A Nylon tube of the desired diameter (43.5 mm) to define the inner diameter of the copper magnet coil was procured. See Figure S4a for image. (b) The tube was covered in a removable layer (e.g., ScotchBlue Painter's Tape, 3M) and a thin layer of grease was applied to this overlayer. The greased tube was wrapped in a thin layer of clear vinyl sheet (0.005" thickness), which was secured in a tube shape using Kapton tape (Polyimide Film Tape 5413, 3M). The grease and vinyl sheet acted in concert to prevent the coil from freezing on to the tube after fabrication. An aluminum bit was optionally machined and secured to the tube to allow for attachment of the tube to a rotating lathe or power drill. See Figure S4b for

images. (c) Two thick sheets of polycarbonate (1/2”) were cut to size, including through holes of the appropriate diameter, and the tube was inserted through these holes. Standard laboratory hose clamps were used to set the maximum distance between the two polycarbonate sheets at the desired coil width (41 mm). See Figure S4c for images. (d) The tube was attached to a rotator (e.g., lathe, power drill, or manual turning). The copper magnet wire was secured to the tube outside of the defined coil area using four hand-wound windings and standard laboratory tape. A single hand winding was done inside the defined coil area and the rest of the copper magnet wire, still wound on the as-received bobbin, was secured such that it could readily feed wire to the growing coil as rotation proceeded. Care was taken to always maintain a taut wire between the copper magnet wire bobbin and the growing copper magnet coil. (e) The tube was rotated through enough rotations as to completely cover the defined coil area with a single layer of copper wire windings. See Figure S4e for images. (f) The single-layer coil was adhered together using cyanoacrylate adhesive and adhesive accelerator. Approximately one minute was allowed to elapse after adhesive applicatoin before continuing the rotation. (g) Windings were added to the coil body as evenly as possible, stopping approximately every 100 winding additions to add a small additional amount of adhesive, until the desired coil size was obtained (here, 1000 total windings). This number can be counted, but can also be approximated by coil weight or resistance. An exact number of windings is not required as small deviations between and amongst magnet coils can be corrected via software or via increased/decreased applied current/voltage. Once the desired number of windings was obtained, an additional layer of adhesive was applied. (h) The hose clamps and polycarbonate sheet were removed from the tube, and the newly fabricated coil was slid off the tube with the vinyl sheet covering. The vinyl sheet is easily removed from the copper magnet coil, and excess magnet wire can be cut to size. Care should be taken not to cut the remaining tail of wire too short, as an electrical connection to a power source is needed. (i) The fabricated copper magnet coil is now ready to use.

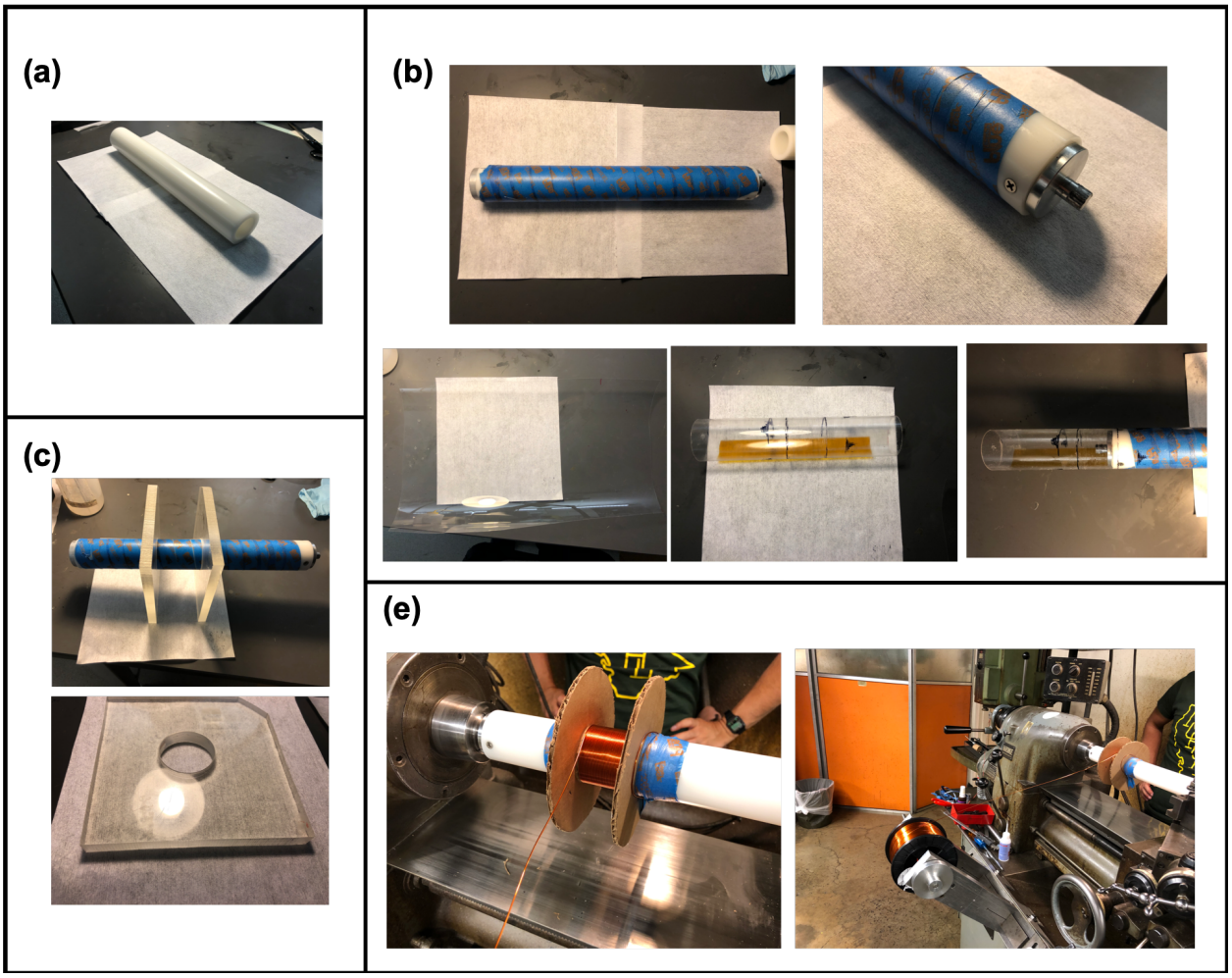

Figure S4: Images of copper magnet coil fabrication. Panels are identified and associated by letter with fabrication steps in Figure S3. (a) Nylon tube to wind copper magnet coil on). (b) *clockwise from top left*, Nylon tube covered in painter's tape and a light coating of grease; aluminum bit used to attach tube to lathe or power drill; vinyl sheet in tube shape half attached to tube; vinyl sheet in tube shape; vinyl sheet as-received. (c) *top to bottom*, polycarbonate sheets on tube prior to hose clamp attachment; polycarbonate sheet cut to size, including through hole. (e) *left to right*, single layer of copper coils on tube while attached to lathe; view of the lathe and copper magnet wire bobbin. Note the polycarbonate fins and hose clamps are not present in these images.

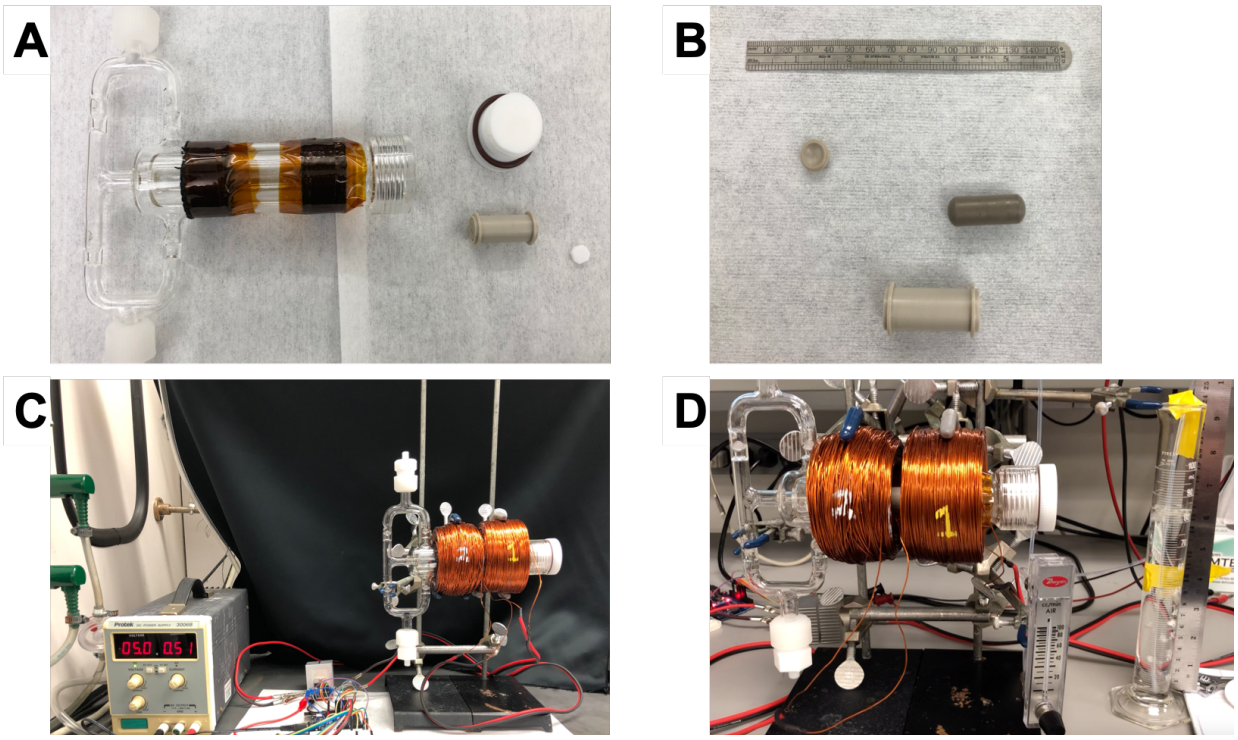

Figure S5 : Images of pump components. (A) Glass pump components: glass pump body with thermal exhaust tape attached using Kapton tape, Ace Thred #25 plug, piston body, and anti-wedge PTFE stopper are visible. Note that the optional custom PTFE stopper rod seen in Figure 1 is not shown here. (B) Piston components: piston screw cap, PEEK-encapsulated stir magnet, and piston body are visible. (C) Glass pump attached to electronic controller: Glass pump inserted into magnet coils (labeled "1" and "2") are visible. (D) Pump under operation at >100 mL min^{-1} flow rate of air (see flowmeter reading) and against an outlet pressure of +6 in. H_2O (see depth of outlet tube in water in the graduated cylinder). A movie of this operation is provided (SI Movie 1).

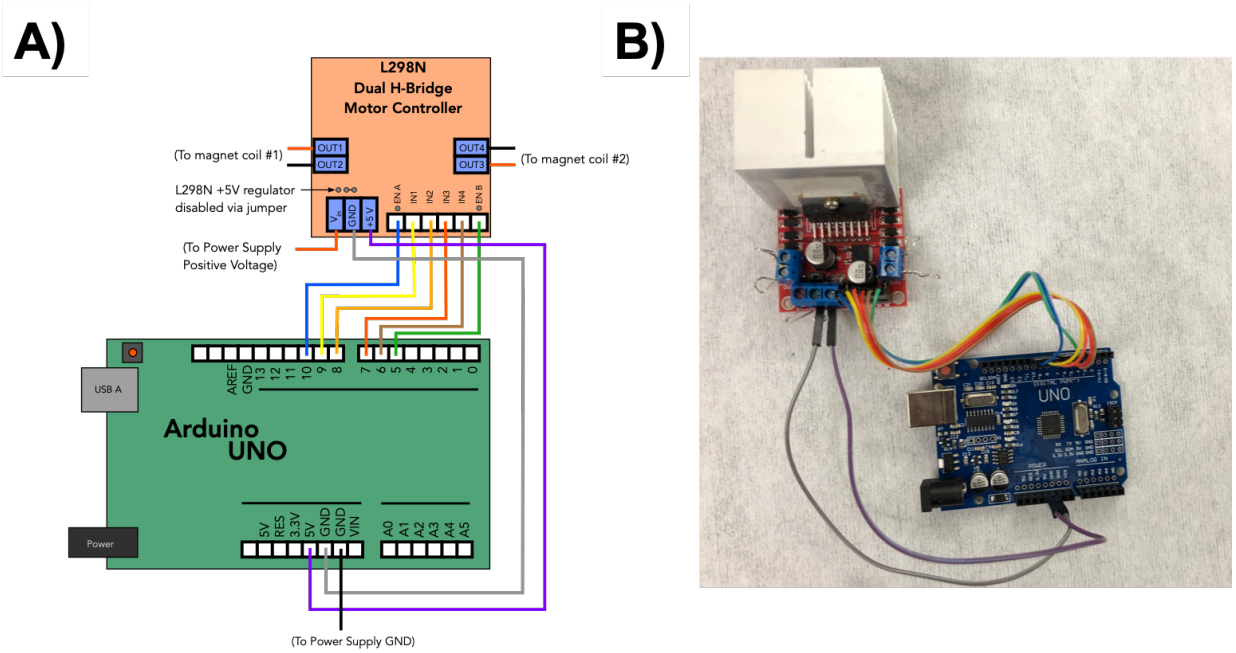

Figure S6: Example wiring for electronic control of glass pump. A) Schematic of wiring connectivity between microcontroller, H-bridge, and magnet coils for glass pump operation. Note that the H-bridge +5V regulator is disabled via jumper selection. Logic voltage for the H-bridge is supplied from the microcontroller. The connectivity of the magnet coils to the H-bridge should be selected for the desired magnetic field directions on application of positive or negative potential. B) Image of the connected H-bridge and microcontroller. The connection to the 3006B Protek power supply and magnet coils are not present in the image. The Arduino UNO microcontroller was powered via the power jack on the board using a center-positive AC-to-DC adapter.

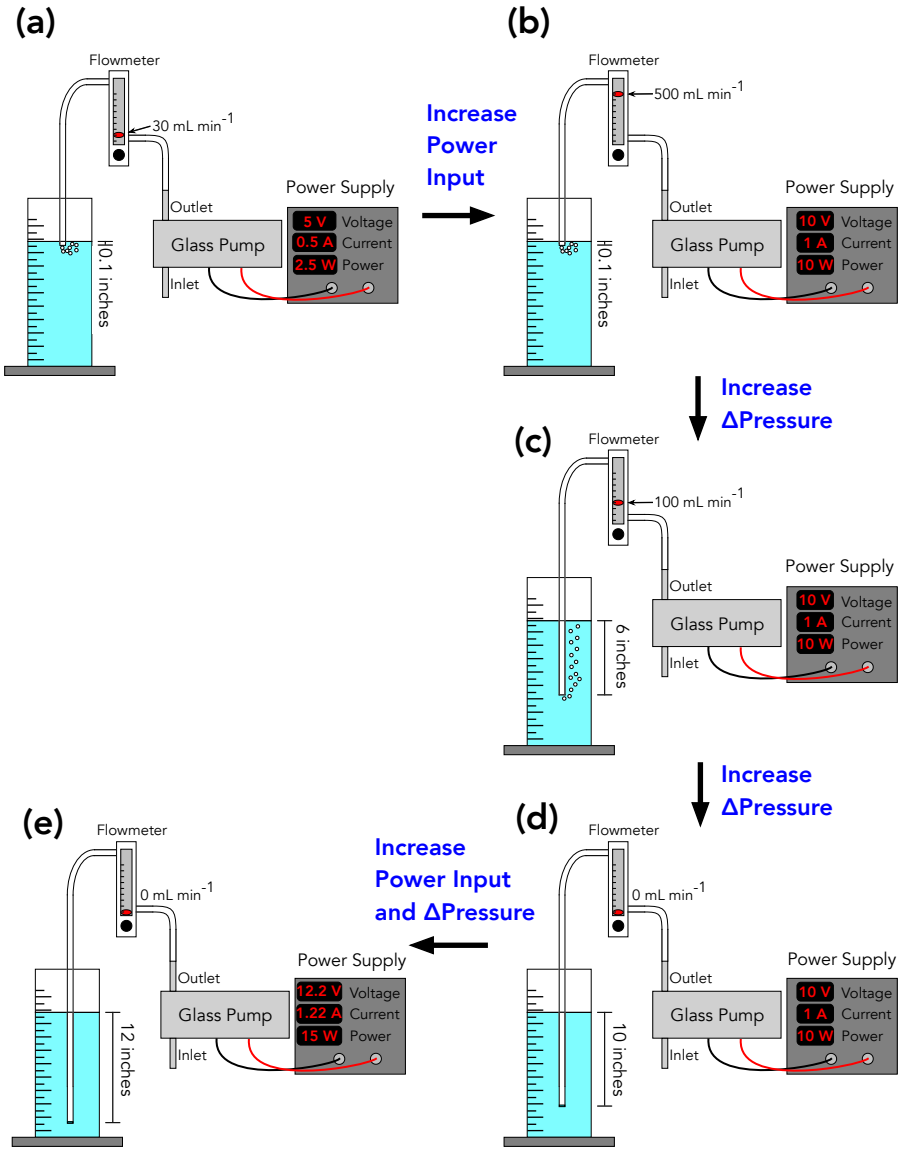

Figure S7: Schematic depiction of the experiment used to obtain the data seen in Table 1. Differential pressure was increased by pushing the outlet tube deeper into a container of water. Power input was controlled using an external power supply. Flow rate was measured as function of these two variables. Panel (a) represents an arbitrary initial condition (see row 1 of Table 1) under which the flow rate is 30 mL min^{-1}, the differential pressure is 0.1 in. H_2O, and the peak power input is 2.5 W. The condition in (b) (see row 2 of Table 1) is achieved by increasing the peak power input and holding the differential pressure constant. Panels (c), (d), and (e) represent the conditions described in Table 1, rows 3, 4, and 5, respectively, and can be achieved by modifying the differential pressure and/or power input.

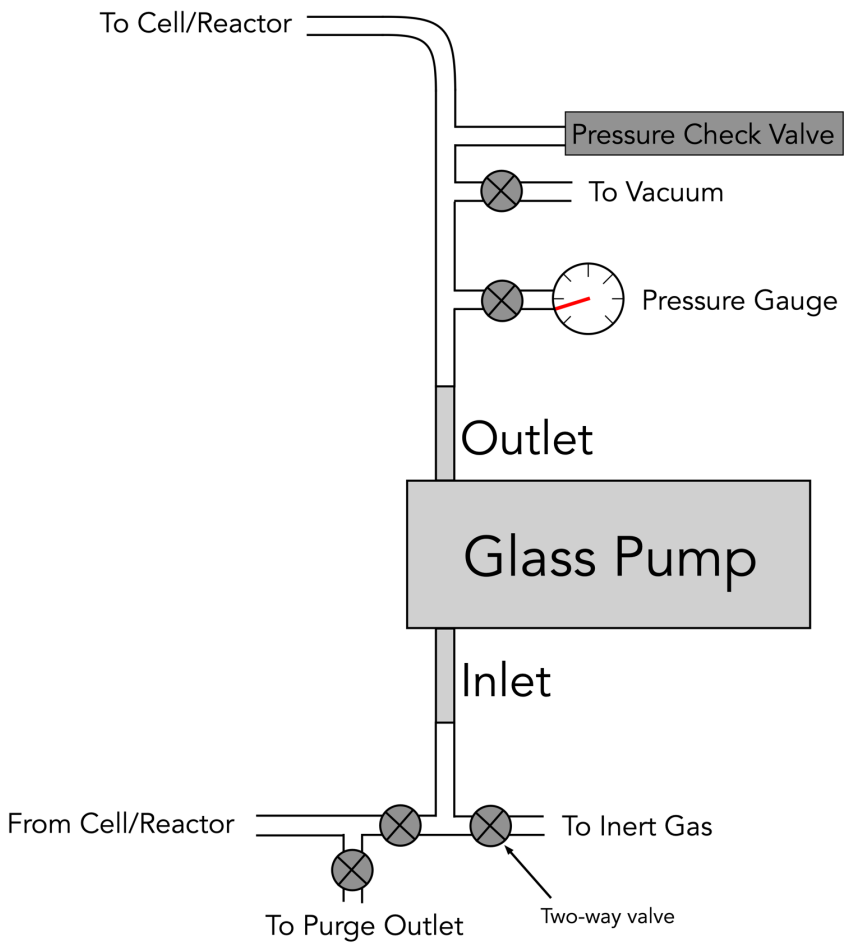

Figure S8: Example schematic for pump evacuation and inert gas purge. All valves are two-way valves and are represented by a gray circle with an 'X'. The reactor was evacuated by attached a vacuum source to the vacuum connection with all valves shut except the vacuum and the pressure gauge valve. The reactor was purged by attaching an inert gas (Ar, N_2) source with the appropriate pressure regulation (e.g., +1 psig) to the inert gas connection and closing all valves except the inert gas valve and the purge valve. A saturator to maintain a constant electrolyte volume level in the electrochemical cell may also be valuable. The cell/reactor can be isolated by additional valving, and purge of only the pump can be achieved by closing all valves except the inert gas valve and the vacuum valve open. A pressure check valve was included as a safety measure to avoid over-pressurization of the system.

Content of: Pump_Controller_No_Ext_Control.txt

```
/*
   https://www.teachmemicro.com/use-l298n-motor-driver/

   https://tronixlabs.com.au/news/tutorial-l298n-dual-solenoid-controller-module-2a-and-arduino/

    DC solenoid 1 "+" or stepper solenoid A+
    DC solenoid 1 "-" or stepper solenoid A-
    12V jumper - remove this if using a supply voltage greater than 12V DC. This
solenoid1ble_solenoid1bles power to the onboard 5V regulator
    Connect your solenoid supply voltage here, maximum of 35V DC. Remove 12V jumper if >12V DC
    GND
    5V output if 12V jumper in place, ideal for powering your Arduino (etc)
    DC solenoid 1 solenoid1ble_solenoid1ble jumper. Leave this in place when using a stepper solenoid.
Connect to PWM output for DC solenoid speed control.
    DC solenoid 2 solenoid1ble_solenoid1ble jumper. Leave this in place when using a stepper solenoid.
Connect to PWM output for DC solenoid speed control.
    DC solenoid 2 "+" or stepper solenoid B+
    DC solenoid 2 "-" or stepper solenoid B-

*/

//Edited 2019 Dec 11 by Adam Nielander.

// set all the solenoid control pins to outputs
#define enable_solenoid1 10   //define  solenoid1 enable   as pin 10.
#define enable_solenoid2 5   //define  solenoid2 enable   as pin 5.
#define in1 9 //pin D9 of arduino, to control H bridge of solenoid 1
#define in2 8  //pin D8 of arduino, to control H bridge of solenoid 1
#define in3 7  //pin D7 of arduino, to control H bridge of solenoid 2
#define in4 6  //pin D6 of arduino, to control H bridge of solenoid 2

void setup()
{
  // All solenoid H bridge control pins are outputs
  pinMode(enable_solenoid1, OUTPUT); //set high to solenoid1ble_solenoid 1, or feed with PWM to
control power/speed
  pinMode(enable_solenoid2, OUTPUT); //set high to solenoid1ble_solenoid 2, or feed with PWM to
control power/speed
  pinMode(in1, OUTPUT); //digital output pin  from arduino  to control  H bridge
  pinMode(in2, OUTPUT); //digital output pin  from arduino  to control  H bridge
  pinMode(in3, OUTPUT); //digital output pin  from arduino  to control  H bridge
  pinMode(in4, OUTPUT); //digital output pin  from arduino  to control  H bridge

  Serial.begin(9600); // initialize the serial communication


}

void loop()
{
    oscillate_piston();
```

```
}


void oscillate_piston() //function to run solenoids
{    delay(500);//  piston travel time in milliseconds delay between the two solenoids
 //  turn on solenoid1  forward, piston to the left
  analogWrite(enable_solenoid1, 255);  //255 indicates 100% duty cycle //analogWrite(0) means a signal
of 0% duty cycle analogWrite(127) means 50% duty cycle
  digitalWrite(in1, HIGH);
  digitalWrite(in2, LOW);

  // turn on solenoid2 reverse
  analogWrite(enable_solenoid2, 255); //reverse solenoid set to lower power to allow forward coil to pull
piston towards itself even if piston is out of position such that reverse coil would otherwise push piston in
incorrect direction
  digitalWrite(in3, HIGH);
  digitalWrite(in4, LOW);

  delay(500);//  piston travel time in milliseconds delay between the two solenoids
  // inverse of previous push-pull combination.
  // turn on solenoid1 reverse piston to the right
  analogWrite(enable_solenoid1, 255);
  digitalWrite(in1, LOW);
  digitalWrite(in2, HIGH);
  // turn on solenoid2 forward
  analogWrite(enable_solenoid2, 255);
  digitalWrite(in3, LOW);
  digitalWrite(in4, HIGH);



}
```

Component *(Subcomponent)*	Description	Manufacturer/Vendor	Vendor Part#	Notes
Glass Pump Body				
Glass pump body	Single-piece glass chassis, piston tube, and check valves. Sealed with Ace Thred #25 PTFE Stopper	Adams & Chittenden Scientific Glass (Berkeley, CA)	n/a	
Magnetic-core Piston				
PEEK Piston Body	Custom fabrication (see schematic for specifications)	n/a (in-house fabrication)	n/a	
Magnetic Core	Magnetic stir bar. 11.5mm diameter, 35.5mm long. Ketron® ClassixTM LSG PEEK encapsulated NdFeB (52 MGO) magnet.	V&P Scientific, Inc (San Diego, CA)	VP 772BK-N52-11-36.1	
Magnet coils				
Magnet wire	20 AWG copper magnet wire	TEMCo Industrial (Fremont, CA)	MW0167	
Adhesive	Starbond Super Fast Thin CA Glue	Starbond (Los Angeles, CA)	EM-02	Used to adhere magnet wire to coil shape
Adhesive accelerant	Adhesive Accelerator 8oz Bottle w/ Sprayer	Partsmaster (Dallas, TX)	DY67051008	
2-conductor zip cord wire	18 AWG 2-conductor power speaker wire	Consolidated Electronic Wire & Cable (Franklin Park, IL)	5176	Used to attach magnet coils to electronic controller
Vinyl sheet	Clear, Chemical Resistant PVC Film	McMaster-Carr	87875K91	0.005" thickness
Nylon tube with aluminum bit	Nylon tube with attached aluminum bit	n/a (in-house fabrication)	n/a	Nylon tube can be acquired from Professional Plastics or McMaster-Carr. Aluminum bit not necessary if tube can be mounted directly on lathe with appropriately-sized chuck
Electronic Controller				
Power supply	Protek Single Output DC Power Supply (60V, 1.5A)	Protek (Tempe, AZ)	3006B	
Microcontroller	Arduino UNO Rev3, ATmega328P	Arduino	8058333490090	
Dual H-bridge	L298N Dual H-bridge Motor Controller module	Amazon.com	B014KMHSW6	Custom heat sink may improve thermal performance
Pump-to-tubing attachments				
PTFE Compression fitting	PTFE Reducing Union (1/2" x 1/8")	Ace Glass (Vineland, NJ)	D167290	Size to desired inlet/outlet tubing diameter
Stainless steel compression fitting	SS Ultra Torr Swagelok Tube Fitting Union (1/2" x 1/2")	Swagelok (Solon, OH)	SS-8-UT-6-810	Size to desired inlet/outlet tubing diameter
Anti-wedge stopper	PTFE sheet (0.250" thick)	Professional Plastics (San Jose, CA)	STFE.250V	Cut to size
PTFE cap stopper (optional)	Threaded PTFE Tube/PTFE Screw	n/a (in-house fabrication)	n/a	PTFE Screw may be purchased instead of in-house fabrication of threaded PTFE tube

Table S1: Components/sub-components recommended for glass piston pump construction. This list is also available in the associated SI .xlsx file (Table _of_Glass_Pump_Components.xlsx).adf

SI References

(1) Andersen, S. Z.; Čolić, V.; Yang, S.; Schwalbe, J. A.; Nielander, A. C.; McEnaney, J. M.; Enemark-Rasmussen, K.; Baker, J. G.; Singh, A. R.; Rohr, B. A.; Statt, M. J.; Blair, S. J.; Mezzavilla, S.; Kibsgaard, J.; Vesborg, P. C. K.; Cargnello, M.; Bent, S. F.; Jaramillo, T. F.; Stephens, I. E. L.; Nørskov, J. K.; Chorkendorff, I. A Rigorous Electrochemical Ammonia Synthesis Protocol with Quantitative Isotope Measurements. *Nature* **2019**, *570*, 504–508.

(2) Rottländer, H.; Umrath, W.; Voss, G. Fundamentals of Leak Detection, Leybold GmbH. In *Catalog No. 199 79_VA.02*; Cologne, Germany, 2016; pp 1–49.

(3) Pasternak, R. A.; Christensen, M. V.; Heller, J. Diffusion and Permeation of Oxygen, Nitrogen, Carbon Dioxide, and Nitrogen Dioxide through Polytetrafluoroethylene. *Macromolecules* **1970**, *3*, 366–371.

(4) O'Hanlon, J. F. Outgassing Rates of Elastomers - Appendix C.4. In *A User's Guide to Vacuum Technology*; John Wiley and Sons: Hoboken, NJ, 2003.

(5) Peacock, R. N. Practical Selection of Elastomer Materials for Vacuum Seals. *J. Vac. Sci. Technol.* **1979**, *17*, 330–336.

(6) Dayton, B. B. Outgassing of Materials - Chapter 4.7. In *Handbook of Vacuum Science and Technology*; Academic Press: San Diego, CA, 1998.

(7) Thieme, G. Mass Spectrometer Investigation of Gas Emission from Plastics. *Vacuum* **1963**, *13*, 137–143.

(8) Barton, R. S.; Govier, R. P. A Mass Spectrometric Study of the Outgassing of Some Elastomers and Plastics. *J. Vac. Sci. Technol.* **1965**, *2*, 113–122.

(9) Callister, W. D.; Rethwisch, D. G. Chapter 5 - Diffusion. In *Materials Science and Engineering - An Introduction*; John Wiley and Sons: Hoboken, NJ, 2014.

(10) Battes, K.; Day, C.; Hauer, V. Outgassing Behavior of Different High-Temperature Resistant Polymers. *J. Vac. Sci. Technol. A Vacuum, Surfaces, Film.* **2018**, *36*, 021602.

(11) Ammonia. *The Merck Index Online*; Royal Society of Chemistry, 2013.

(12) Habibzadeh, F.; Miller, S. L.; Hamann, T. W.; Smith, M. R. Homogeneous Electrocatalytic Oxidation of Ammonia to N 2 under Mild Conditions. *Proc. Natl. Acad. Sci.* **2019**, *116*, 2849–2853.

(13) Appl, M. Ammonia, 2. Production Processes. In *Ullmann's Encyclopedia of Industrial Chemistry*; Wiley-VCH Verlag GmbH & Co. KGaA, 2000.

(14) Hirscher, M.; Yartys, V. A.; Baricco, M.; Bellosta von Colbe, J.; Blanchard, D.; Bowman, R. C.; Broom, D. P.; Buckley, C. E.; Chang, F.; Chen, P.; Cho, Y. W.; Crivello, J. C.; Cuevas, F.; David, W. I. F.; de Jongh, P. E.; Denys, R. V.; Dornheim, M.; Felderhoff, M.; Filinchuk, Y.; Froudakis, G. E.; Grant, D. M.; Gray, E. M. A.; Hauback, B. C.; He, T.; Humphries, T. D.; Jensen, T. R.; Kim, S.; Kojima, Y.; Latroche, M.; Li, H. W.; Lototskyy, M. V.; Makepeace, J. W.; Møller, K. T.; Naheed, L.; Ngene, P.; Noréus, D.; Nygård, M. M.; Orimo, S. ichi; Paskevicius, M.; Pasquini, L.; Ravnsbæk, D. B.; Veronica Sofianos, M.; Udovic, T. J.; Vegge, T.; Walker, G. S.; Webb, C. J.; Weidenthaler, C.; Zlotea, C. Materials for Hydrogen-Based Energy Storage – Past, Recent Progress and Future Outlook. *J.*

Alloys Compd. **2020**, *827*.
(15) Ockwig, N. W.; Nenoff, T. M. Membranes for Hydrogen Separation. *Chem. Rev.* **2007**, *107*, 4078–4110.
(16) Grashoff, G. J.; Pilkington, C. E.; Corti, C. W. The Purification of Hydrogen l Johnson Matthey Technology Review. *Platin. Met. Rev.* **1983**, 157–169.
(17) Sakamoto, F.; Kinari, Y.; Chen, F. L.; Sakamoto, Y. Hydrogen Permeation through Palladium Alloy Membranes in Mixture Gases of 10% Nitrogen and Ammonia in the Hydrogen. *Int. J. Hydrogen Energy* **1997**, *22*, 369–375.
(18) Musket, R. G. Effects of Contamination on the Interaction of Hydrogen Gas with Palladium: A Review. *J. Less-Common Met.* **1976**, *45*, 173–183.
(19) Wolf, R. J.; Lee, M. W.; Davis, R. C.; Fay, P. J.; Ray, J. R. Pressure-Composition Isotherms for Palladium Hydride. *Phys. Rev. B* **1993**, *48*, 12415–12418.
(20) Sakai, T.; Oguro, K.; Miyamura, H.; Kuriyama, N.; Kato, A.; Ishikawa, H.; Iwakura, C. Some Factors Affecting the Cycle Lives of LaNi5-Based Alloy Electrodes of Hydrogen Batteries. *J. Less-Common Met.* **1990**, *161*, 193–202.
(21) Auer, W.; Grabke, H. J. The Kinetics of Hydrogen Absorption in Palladium (α- and β-Phase) and Palladium-Silver-Alloys. *Berichte der Bunsengesellschaft für Phys. Chemie* **1974**, *78*, 58–67.
(22) Sheridan, J. J.; Eisenberg, F. G.; Greskovich, E. J.; Sandrock, G. D.; Huston, E. L. Hydrogen Separation from Mixed Gas Streams Using Reversible Metal Hydrides. *J. Less-Common Met.* **1983**, *89*, 447–455.
(23) Robeson, L. M. Correlation of Separation Factor versus Permeability for Polymeric Membranes. *J. Memb. Sci.* **1991**, *62*, 165–185.
(24) Marchese, J.; Ochoa, N.; Pagliero, C. Preparation and Gas Separation Performance of Silicone-coated Polysulfone Membranes. *J. Chem. Technol. Biotechnol.* **1995**, *63*, 329–336.